RSC Advances

ROYAL SOCIETY OF CHEMISTRY

www.rsc.org/advances

P-doped carbon dots act as nanosensor for trace 2,4,6-trinitrophenol detection and fluorescent reagent for biological imaging

Dechao Shi [a], Fanyong Yan [a*], Tancheng Zheng [a], Yinyin Wang [b], Xuguang Zhou [a**], Li Chen [a]

[a] *State Key Laboratory of Hollow Fiber Membrane Materials and Processes, Key Lab of Fiber Modification & Functional Fiber of Tianjin, Tianjin Polytechnic University, Tianjin 300387, PR. China*

[b] *TianJin Engineering Center for Safety Evaluation of Water Quality & Safeguards Technology, PR. China*

[*] Corresponding author. Tel.: +86 22 83955766; fax: +86 22 83955766
E-mail address: yfany@163.com (F.Y. Yan).
[**] Corresponding author. *E-mail address:* xaodayin@sohu.com (X.G. Zhou).

ABSTRACT

A simple and rapid method for sensitive and selective detection of 2,4,6-trinitrophenol (TNP) was developed with the use of water-soluble carbon dots (CDs) as a nanosensor. The CDs with a fluorescence quantum yield of 21.8% are easily prepared by hydrothermal treatment of sucrose phosphate solution. In this sensing system, the fluorescence of CDs would be significantly quenched by TNP, while other nitroaromatic derivatives and common reagents exhibited little influence on the detection of TNP. The efficient selective detection of TNP can be attributed to the fluorescence resonance energy transfer process (FRET). This phenomenon can be used for the selective sensing of TNP with a limit of detection of 16.9 nM and a linear range of 0.2-17.0 μM. The recovery result for TNP in real samples by this assay method was satisfying, demonstrating its potential application as fluorescence sensor. Furthermore, the resulting CDs solution could replace traditional colorings and was successfully applied for Escherichia coli labeling and intracellular imaging.

Keywords: Carbon dots; Fluorescence sensor; 2,4,6-Trinitrophenol; Bacterial labeling; Intracellular imaging.

Introduction

Ever-increasing concerns of national security and public safety have increased a wide interest in developing sensitive and rapid methods for detection of high explosives, especially 2,4,6-Trinitrophenol (TNP), due to their importance in homeland security, environmental and health-care issues [1-5]. 2,4,6-Trinitrophenol (TNP), a common reagent and representative nitroaromatic, has been firstly synthesized and used as military explosive with strong explosion ability and low safety coefficient [6-9]. Besides, it has widely applications in dyes, fireworks, leather and medicine industry [10-13]. In addition to serious environmental pollution caused by TNP extensively existing in the soil and ground water near military and industrial facilities, the careless inhale, ingest or touch of TNP by living organisms may cause skin irritation, liver or kidney damage, cyanosis and aplastic anemia, especially human beings [14-19]. In view of the significance of TNP, it is highly desired to develop simple analytical methods, especially an effective and selective sensor, for detecting trace amounts of TNP.

Up to now, numerous techniques and protocols, such as surface enhanced Raman spectrometry, high-pressure liquid chromatography, and electrochemical methods, have been well developed and utilized to monitor nitroaromatic explosives [2,20]. However, these methods suffer from several limitations, which greatly limit their practical applications, such as high-cost, less sensitive and low anti-interference ability [21]. Recently, fluorescence-based detection methods by utilizing photoluminescent polymers, small organic molecules, nanomaterials and

semiconductor quantum dots (QDs) has drawn much attention owing to its sensitivity, short response time and convenient visual detection [22-26]. Unfortunately, the above-mentioned strategies suffers from low photo-stability and complex synthesis process, while the application of QDs is limited since the serious health and environmental concerns caused by heavy metals. Therefore, searching for excellent fluorescence sensing materials that can overcome the above limitations are highly desirable.

Carbon dots (CDs), a new class of brightly photoluminescent nanomaterials with their photophysical properties resemble in many respects those commonly found in QDs, recently attracted a great deal of attention owing to their optical properties [27-32]. Compared to the conventional heavy-metal-based QDs and organic fluorescent dyes, CDs have generated enormous excitements because of their superiority in water solubility, good biocompatibility, low-toxicity, low cost, high photo-stability and ease of functionalization [33-36]. In particular, based on their strong and tuneable photoluminescence and biocompatible properties, carbon dot-based nanosensors were successfully implemented in biological imaging and detection areas [37-42]. Various synthetic approaches, including chemical ablation [33,43], electrochemical etching [44], microwave irradiation [45,46], ultrasonic [47] and hydrothermal/solvothermal treatment methods [48,49], have been extensively explored to prepare CDs. Among them, the hydrothermal treatment of biomass has been reported to be effective for the production of CDs groups. Regrettably, less effort has been focused on developing green methods for detecting nitroaromatic explosives,

especially TNP, although it is important to homeland security, environment and health-care issues [50,51].

In addition, detection and microscopic visualization of bacteria are of vital important in clinical diagnosis, infectious diseases prevention as well as public health and safety. Traditional methods for the detection of bacteria generally rely on indirect detection of bacterially-secreted metabolites or visualization of bacterial colonies, while the imaging approaches mainly depend on the use of varied staining techniques using either fluorescence dyes or semiconductor quantum dots [52-54]. However, these strategies widely used commercially agents and operation process is laborious and time-consuming. There is still a need for versatile platforms that would be technically simple and inexpensive and would provide morphological details on bacterial cells. Amphiphilic CDs, derived from varied molecular residues, can be employed as useful fluorescent probes for membrane analysis. Moreover, amphiphilic CDs exhibit high affinity to actual cellular membranes, which enabling multicolor microscopic imaging of cells and intracellular organelles [55]. Herein, the amphiphilic CDs were explored to serve as effective fluorescent markers of bacterial cells.

In this case, we explored a simple and low toxicity method using CDs as a type of water-soluble fluorescent probe for highly selective and sensitive detection of TNP in aqueous solution. Due to the highly electron deficient and strong light absorption characteristics of TNP, CDs with rich electron-donor groups can significantly enhance the interaction between CDs and TNP through electron transfer mechanism, and then fluorescence quenching of CDs might be occurred for detecting TNP with high

efficiency and selectivity. In the other hand, the maximum absorption band of TNP may overlap with the fluorescence emission band of CDs, which gives rise to the fluorescence resonance energy transfer (FRET). Based on later mechanism, we synthesized hydroxyl-rich CDs through the hydrothermal carbonization of phosphoric acid solution of sucrose. As the result, CDs with uniformly spherical morphology and narrow size distribution with the diameters ranging from 1.2 to 5.0 nm were obtained. They exhibited excellent function of highly selective and sensitive detecting trace amounts of TNP in aqueous solution via fluorescence resonance energy transfer process between TNP and CDs, which expanding the potential applications of these fluorescent nanoparticles in the detection of nitroaromatic explosives. Moreover, the resulting CDs were shown to exhibit high affinity to actual cellular membranes, and successfully serve as effective fluorescent markers of biological cells.

Experimental

Chemicals and apparatus

Sucrose and phosphoric acid were analytical grade and purchased from the local company. Quinine sulfate (99%, suitable for fluorescence) was supplied by Aladdin. Phosphate buffered saline (PBS) was purchased from Sigma-Aldrich. All other chemicals were of analytical grade and used as received without any further purification. A tris (0.2 mol L^{-1})−HCl (0.1 mol L^{-1}) buffer solution was used to maintain the pH of the solutions at 7.0. Dialysis bags (MWCO=1000) were purchased from Millipore Corporation (Billerica, USA). The deionized water obtained from a

Millipore NanoPure purification system (resistivity higher than 18.2 MΩcm^{-1}) was used in all experiments.

High-resolution TEM (HRTEM) measurements were carried out using a JEOL JEM 2011 microscope at an acceleration voltage of 200 kV. The specimen was prepared by drop casting the sample dispersion onto a carbon-coated copper grid and drying at room temperature. The absorption spectra were measured on a UV–vis spectrometer (Purkinje, General TU-1901). Fluorescence spectra were obtained by an F-380 fluorescence spectrophotometer with the excitation wavelength of 310 nm. The Fourier transform infrared (FT-IR) spectra were recorded on a TENSOR37 Fourier transform infrared spectrometer within the range of 400-4000 cm^{-1}. The XPS spectra measurements were performed on an X-ray photoelectron spectroscopy (EDAX, GENESIS 60S). A PHS-3W pH meter was utilized to measure the pH values of aqueous solutions. The fluorescence imaging was observed under an OlympusIX71 inverted fluorescence microscope with a 20× objective lens.

CDs synthesis

The CDs were synthesized by a solvothermal treatment method according to the literature with some modifications [46]. Sucrose (1.5 g) was added into 1.0 mol·L^{-1} phosphoric acid to yield 30 mL transparent solution. Then the solution was transferred to a Teflon-equipped stainless steel autoclave and hydrothermal treatment for 5 h at 200^{o}C in a drying oven. After reaction finished, the autoclave was cooled to room temperature. After centrifuged at 10,000 rpm for 10 min to remove large insoluble particles, sodium hydroxide was added into the aqueous solution to adjust the pH to

neutral. Then, the CDs solution was further purified by dialyzing against de-ionized water using a membrane with 1000 MWCO for 24 h. Thus, the purified homogeneous CDs solution was obtained.

Experimental details for fluorescent sensing

The quenching effect of TNP on the fluorescence intensity of CDs was examined. In a typical process for the detection of TNP, 100 μL of the CDs solution (0.01 mg mL^{-1}) were added to 10 mL volumetric flasks, then TNP solution (10^{-3} $mol \cdot L^{-1}$) ranging from 0 to 200 μL were added and constant volume with double distilled water. For comparison, 100 μL of different phenols and nitrophenols (10^{-3} $mol \cdot L^{-1}$) were added to the volumetric flasks containing CDs solution. The as-produced samples were finally placed at room temperature for an appropriate period of time. The interference of above potential competitors was also studied. A series of sample solutions containing Bisphenol A (BPA), Catechol (Cat), 3,5-Dimethylphenol (Dim), Hydroquinone (Hyd), o-Nitrophenol (o-Nit), Phenol (Phe), Phloroglucinol (Phl), Resorcinol (Res) and 2,4,6-Trinitrotoluene (TNT) were added respectively to 10 mL volumetric flasks with 100 μL of the CDs solution (0.01 mg mL^{-1}). Then, these solutions were titrated by adding 100 μL TNP solution (10^{-3} $mol \cdot L^{-1}$) with trace syringe. These solutions were allowed to stand for an appropriate period of time to equilibrate, and the intensity was recorded.

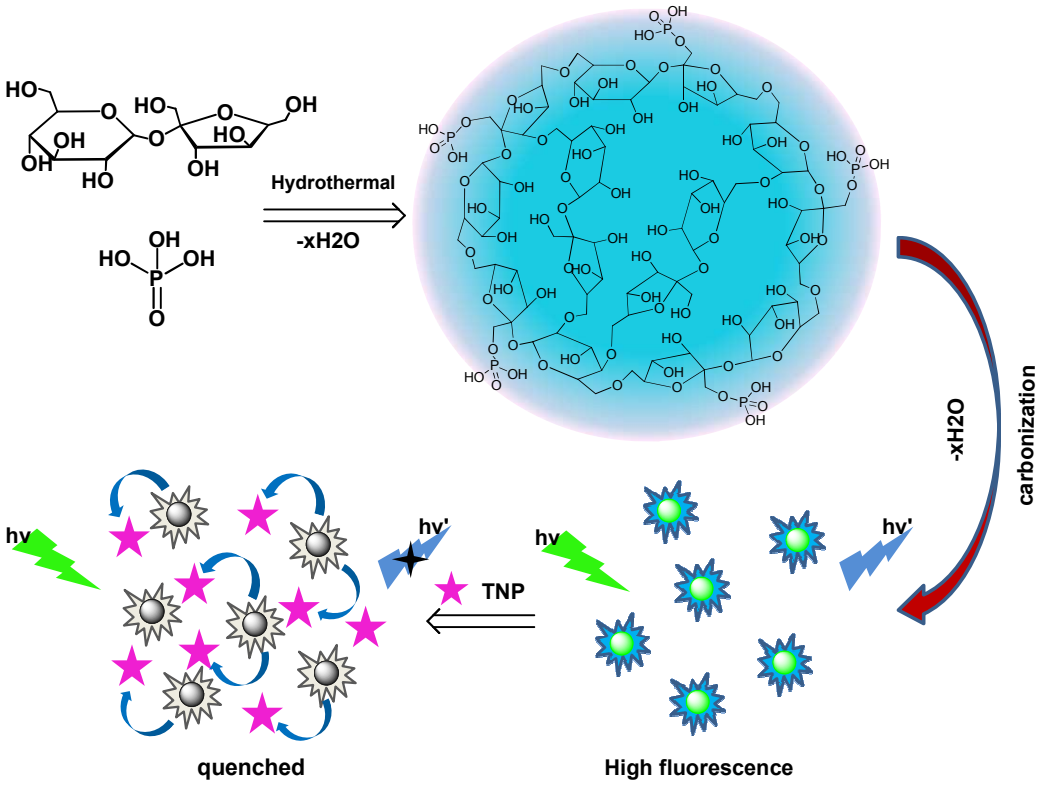

Scheme 1 Synthesis of and fluorescence sensing with CDs.

Results and discussion

Characterization of CDs

The CDs, after dialysis, are uniform, mono-disperse and near spherical with an average diameter of 3.2 nm, as shown in Fig. 1(a). The number distribution showed in insert reveals that the particle size distribution of CDs is between 1.2 and 5.0 nm. FTIR spectra were used to identify the functional groups presented on CDs. As revealed in Fig. 1(b), an apparent absorption peak at about 3117 cm^{-1} might ascribe to the O-H vibration stretch of carboxylic moiety, and the shoulder at 1654 cm^{-1} to C=O vibration. Simultaneously, the absorption band of C=C stretching vibration appeared at 1534 cm^{-1} with the symmetric and asymmetric stretching vibrations of C-O-C

located in the range of 1000-1400 cm^{-1}.

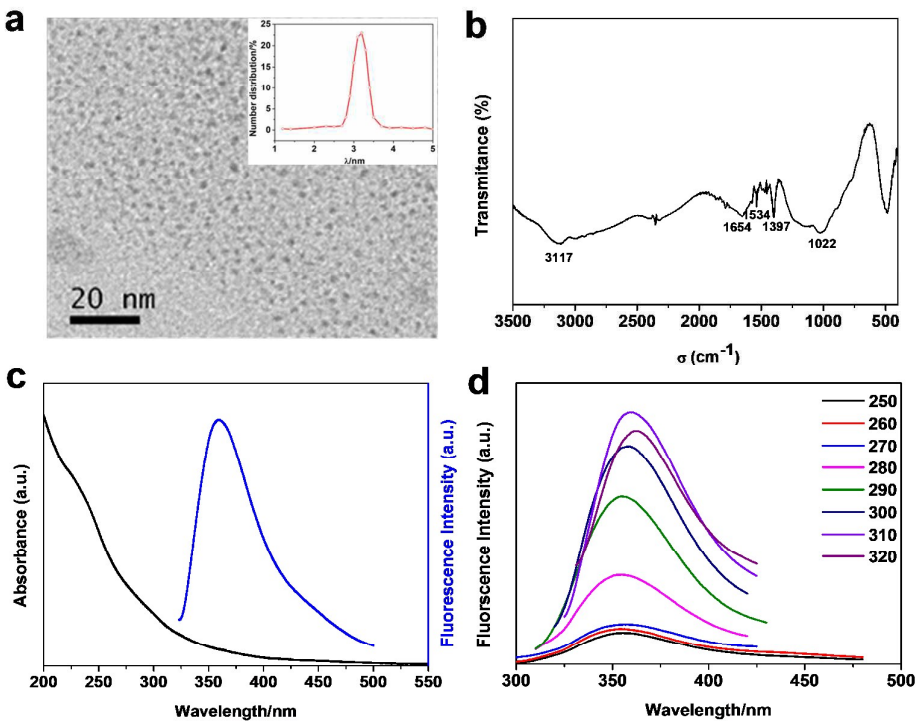

Fig. 1 (a) TEM image of CDs (inset: the diameter distribution of CDs); (b) FTIR spectrum of the as-prepared CDs; (c) UV–vis absorption and fluorescence emission spectra for the CDs; (d) Fluorescence emission spectra of CDs with variations of excitation wavelength.

The optical properties of the as-prepared CDs dispersed in water are shown in Fig. 1(c), (d). Note that no obvious absorption band can be observed in the UV-vis absorption spectrum, like most luminescent CDs [56,57]. A strong fluorescence emission peak centered at 358 nm is observed upon excitation at 310 nm, indicating that the CDs are fluorescent. The quantum yield is determined to be 21.8% with quinine sulfate as a reference (see Supplementary Information, Fig. S3 and Table S1). It is a common phenomenon, observed in carbon-based quantum dots, that the

excitation wavelength dependence of the emission wavelength and intensity. To address whether the synthesis of CDs showed excitation-dependent emission character or not, the fluorescence intensity were recorded upon various excitation wavelengths from 250 nm to 320 nm on the left in 10 nm increments. As shown in Fig. 1(d), the emission peak position shifts to longer wavelengths with the increase of excitation wavelength. The maximum fluorescence emission intensity can be obtained when it is excited at 310nm. Thus, the 310 nm was chosen as the optimal excitation wavelength for the followed detection experiments.

To further confirm the fluorescence stability of CDs, the influences of temperature, irradiation time, ionic strength, pH value on the fluorescence intensity were evaluated. Fig. S1(a) showed the influence of different temperatures on the fluorescence intensity of CDs. It is clear that the fluorescence intensity of CDs kept stable when the temperature increased from 10 to 50 ^{o}C, which indicated that temperature had a little effect on the character of CDs. Then, the photo-stability of CDs was investigated by means of irradiating the obtained CDs under UV light for 6 h. The results showed in Fig. S1(b) suggested that the fluorescence intensity of CDs had no obvious change during this process, which indicated that CDs have good photo-stability. The effect of ionic strength on the fluorescence intensity was tested by adding different concentration of NaCl solutions (from 0.1 to 3.0 mol·L^{-1}) into CDs aqueous solution at room temperature. As shown in Fig. S1(c), the fluorescence intensity of CDs still keep stable, even in aqueous solution with a high ionic strength. The fluorescence intensity of CDs increased firstly and subsequently decreased when

the pH of solution was changed from 2.0 to 9.0, which indicated that CDs was sensitive under neutral environment. From above results, it is can be concluded that the CDs possess high stability, which makes it profoundly suitable for fluorescent detection.

Fluorescence detection of TNP and sensing mechanism

We explored the feasibility of using CDs for TNP sensing in aqueous solution through a solution state fluorescence quenching experiment. Fig. 2 depicts the fluorescence spectra of CDs and CDs-TNP under the same experimental conditions. The CDs in the absence of TNP exhibit a strong excimer emission band at 382 nm with an excitation wavelength of 310 nm. When TNP was added into the solution, it is clear to observe that the strong fluorescence emission of CDs can be quenched obviously. However, the addition of TNP had no effect on the fluorescence wavelength. It also can be seen from Fig. 2 that the fluorescence intensity of CDs was quenched about 50% within 1 min of the contact time, which meant that the response rate was rapid, implying a promising application in a fast sensing of TNP without strict time control.

The special selectivity of CDs for TNP can be understood from the standpoint of FRET from fluorescent CDs and TNP in water. It can be clearly seen from Fig. 3 that the maximum absorption band of TNP centered at 350 nm, which overlaps the fluorescence spectra of fluorescent CDs of appeared at 358 nm, which gives rise to a resonant energy transfer process. As the TNP does not exhibit fluorescence, thus only the fluorescence quenching of CDs can be observed (Scheme 2). To investigate the FRET mechanism of the proposed fluorescence method for TNP detection, we

calculated the overlap integral (J) and the Förster distance (R_0). According to the Förster nonradiative energy transfer theory, Förster radius R_0, the critical distance between donor and acceptor at a transfer efficiency of 50%, was expressed as follows Eq. (1) in angstroms (Å):

$$R_0 = 0.2108 \times [K^2 \times \Phi_D \times n_R^{-4} \times J(\lambda)]^{1/6} \qquad (1)$$

where K^2 is the factor describing the relative orientation of the donor to the acceptor molecule, assumed to be $K^2=2/3$ for dynamic random averaging of the donor and acceptor; n_R is the refractive index of the medium, and Φ_D is the quantum yield of the donor. J(λ) is the overlap integral of the fluorescence emission spectrum of the donor and the absorption spectrum of the acceptor, which can be calculated by use of the following Eq. (2):

$$J(\lambda) = \int_0^\infty F_D(\lambda)\varepsilon_A(\lambda)\lambda^4 d\lambda \qquad (2)$$

$F_D(\lambda)$ is the normalized fluorescence intensity of the donor in the absence of acceptor; $\varepsilon_A(\lambda)$ is molar extinction coefficient of the acceptor, and λ is wavelength. With this data and the molar-extinction coefficient (ε) of TNP, J was calculated to be 7.27×10^{-14} mol^{-1} L cm^{-1} cm^4 in water. From this J value and using Eq. (1), the R_0 value was determined to be 9.8 nm when FRET efficiency is 50 %, which is in accordance with the theory of FRET.

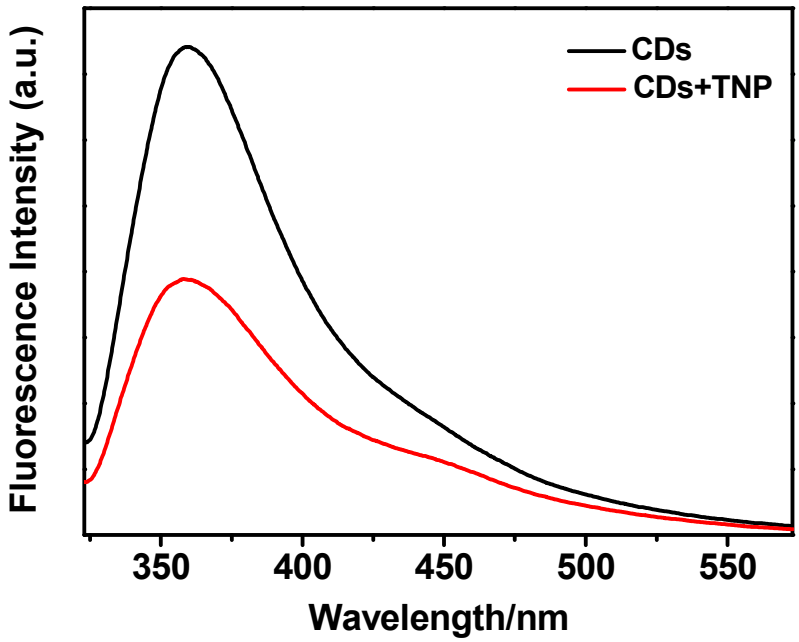

Fig. 2. Fluorescence spectra (λ_{ex}=310 nm) of CDs aqueous solutions in the absence and present of TNP within 1 min.

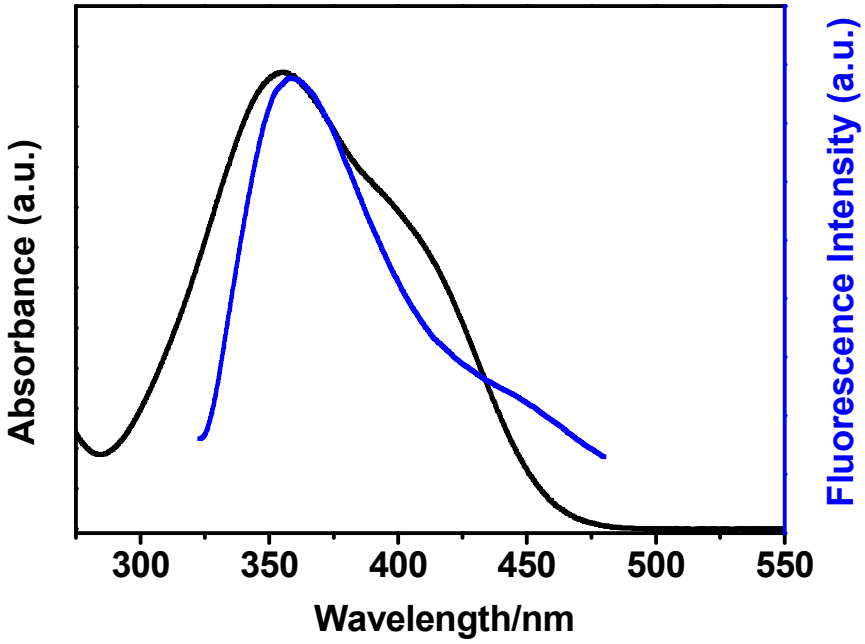

Fig. 3. The fluorescence emission spectra of CDs and absorption spectra of TNP.

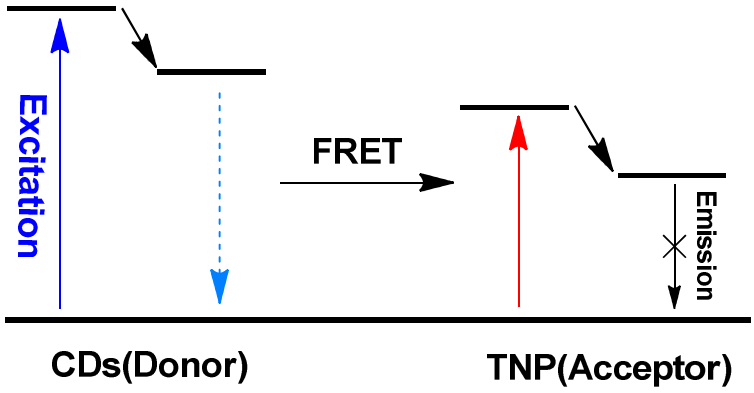

Scheme 2 The mechanism of the fluorescence resonance energy transfer process.

To evaluate the selectivity of the CDs based detection system, the sensing properties of CDs for TNP and common interferents were investigated. Fig. 4 shows the changes of fluorescence intensity of CDs occurred with TNP and potential

interfering substances. It is easy to see that only TNP caused remarkable fluorescence quenching, while other substances have little effect upon the fluorescence emission of CDs. Simultaneously, the interference of above potential competitors was also studied. Fig. 5 clearly showed that even at 20 times higher concentrations than that of TNP, these potential interfering substances exhibited little influence on TNP detection. Above results clearly demonstrate that the proposed CDs possess outstanding selectivity for TNP and can serve as novel fluorescence sensor for highly selective and reliable TNP monitoring.

To improve the performance of CDs sensor for TNP, we optimized the detection conditions, such as the reaction time and pH value, before quantitative analysis of TNP using the proposed method. After the addition of 10 μM TNP, the fluorescence intensity of CDs was recorded every time. As shown in Fig. S2(a), the quenching effect reached maximum within 1 min, and then remained constant over the next reaction time, indicating that a rapid and stable sensor for TNP could be constructed. The pH may have a significant influence on the fluorescence intensity of CDs, and thus, the effect of pH on the reaction system was also tested. A series of PBS buffer with different pH were prepared, and then, the CDs' solution together with 10 μM TNP were added. The fluorescence intensity decreased on addition of TNP at each pH value. However, the maximum value of quenching rate appeared when pH was adjusted to 6.5 (Fig. S2(b)). This implied that the best quenching effect occurred at pH=6.5. Thus, considering the above results, the reaction time and working pH for a sufficiently sensitive and stable sensor for TNP were set to 10 min and 6.5,

respectively.

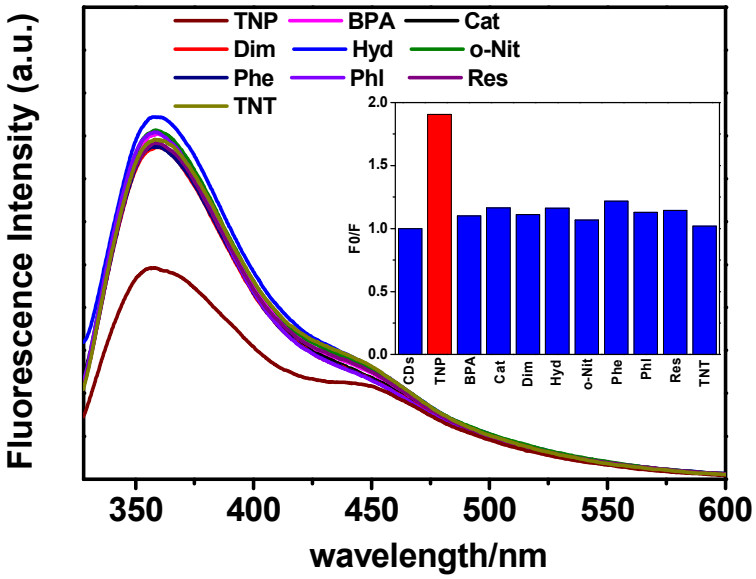

Fig. 4. Fluorescence responses of CDs aqueous solutions (100 μL, 0.01 mg mL^{-1}) in the absence and presence of various contents of analytes (100 μL, 10^{-3} $mol \cdot L^{-1}$) (λ_{ex}=310 nm).

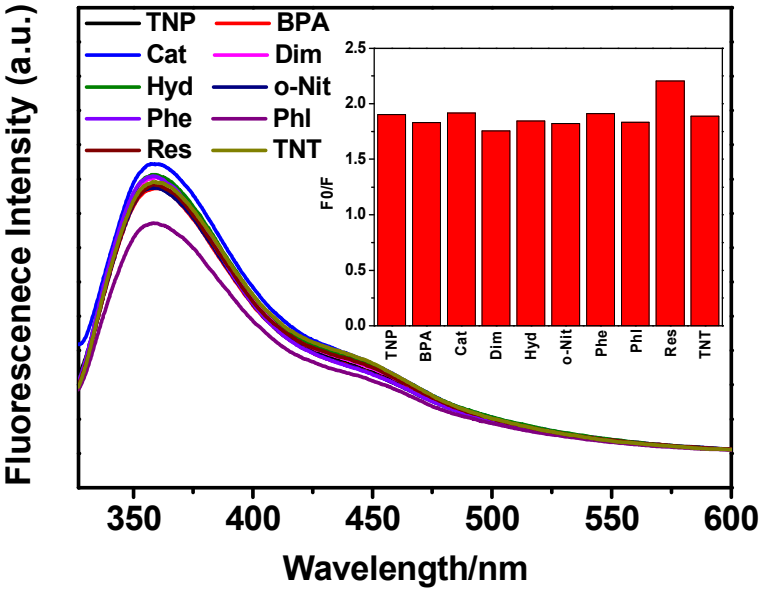

Fig. 5. Interference study of using CDs (100 μL, 0.01 mg mL^{-1}) as sensor for TNP premixed with other potential interfering substances (100 μL, 10^{-3} $mol \cdot L^{-1}$) (λ_{ex}=310 nm).

Under the optimized conditions, the sensitivity of the proposed method was evaluated through fluorescence titration experiments performed by adding of various concentrations of TNP to CDs with a fixed concentration. As previously noted, CDs emit fluorescence at 385 nm (F_0), and TNP quenched this emission in accordance with an energy transfer mechanism. Fig. 6 shows the quenched fluorescence intensity of CDs on different concentration of TNP after reaction for 10 min. It is obvious that the fluorescence intensity of the mixture decreases with the increase of TNP concentration. Correspondingly, the ratio F0/F of normalized fluorescence intensity of CDs proportional increased to the different TNP concentration. TNP quenches the fluorescence of CDs, and thus, a linear calibration may be obtained between the quenched fluorescence intensity and the concentration of TNP, which makes TNP be analyzed quantitatively. Consequently, in the concentration range of 0.2-17.0 μM TNP, the relative fluorescent intensity (F0/F) of CDs could be described by the Stern-Volmer plot with a perfect linear behavior. The calibration curve can be expressed as F0/F=0.081c+0.991 with a correlation coefficient (R^2) of 0.9968. The detection limit for TNP was obtained of 16.9 nM calculated based on 3σ/s (σ is the standard deviation of eight blank measurements, and s is the slope of the calibration curve), which is comparable or even better than those reported parameters in the literatures (shown in Table 1). The results demonstrated the reliability of CDs as an excellent candidate for the determination of sub-micromolar concentration TNP.

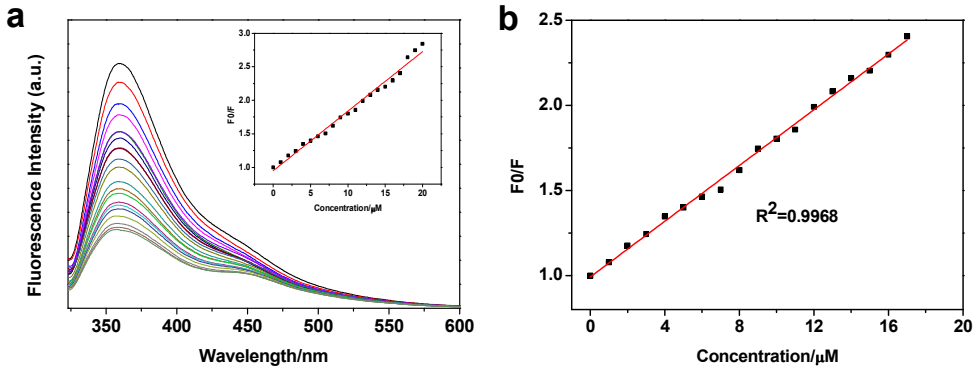

Fig. 6. (a) Fluorescence emission spectra of CDs in the presence of TNP with different concentrations (0-20 μM). Insert: Plots of the values of F0/F at 358 nm versus the concentration of TNP. (b) A linear relationship between F0/F and TNP concentration from 0.2 to 17.0 μM with a correlation coefficient R^2=0.9968 (λ_{ex}=310 nm).

Table 1
Comparison of different methods for detection of TNP.

Methods	Linear range	Detection limit	Reference
Fluorescent copper nanoclusters	0.8-100 μM	120 nM	[2]
Fluorescent metal-organic framework	—	2.6 μM	[23]
Pentacenequinone derivative	2.2-35.0 μM	2.2 μM	[25]
P-doped carbon dots	0.2-17.0 μM	16.9 nM	This work

Applications

To evaluate the practicality of the proposed method, the CDs-based sensor was applied for TNP detection in real samples, which were collected from Haihe River and different pools in Tianjin Polytechnic University. The water samples were spiked with standard solutions containing different concentration of TNP. As mentioned above, the present approach provides a linear response to TNP at concentrations over the range from 0.2-17.0 μM. The analytical results for the water samples spiked with certain amounts standard TNP are given in Table 2. The good recoveries ranging from 92.6% to 108.2% were obtained with a RSD (relative standard deviation) of about 3.17%, which definitely demonstrated that numerous ions and organics existing in water caused little interference with the detection of TNP and the accuracy and reliability of the CDs-based fluorescent sensor for detecting TNP in practical applications.

Moreover, CDs were successfully applied as fluorescence colorings for bacterial labeling, which relied upon incubation of bacteria with the obtained CDs. After subsequent washing, CDs attached to the bacterial cells render them highly fluorescent. To expand the CDs patterns beyond a single fluorescent color in the patterns, the fluorescent imaging were conducted in the absence and presence of TNP, respectively. The image in Fig. 7(a) indicates that the bacterial cells labeled with CDs emit bright blue fluorescence in the presence of TNP. Due to the quenching effect of TNP toward CDs, the bacterial strain shows relatively weak fluorescence after the further incubation of above bacterial cells with PBS solution of TNP (Fig. 7(b)). This new CD-labelling approach opens interesting avenues for bacterial detection applications. Similarly, bioimaging applications of CDs in living NIH-3T3 cells were

then carried out. After the cells were incubated with CDs (10 μM) in culture medium for 30 min at 37 ^{o}C, and bright blue fluorescence of CDs inside the living NIH-3T3 cells was observed (Fig. 8b). After three times washing with PBS buffer, the cells were then supplemented with 10 μM TNP in the growth medium for another 30 min, an obvious fluorescence quenching can be seen from within the cell (Fig. 8d). A bright-field transmission image of cells treated with CDs and TNP confirmed that the cells were viable throughout the imaging experiments (Fig. 8a, c). Thus, above results proven that CDs is cell-permeable and primarily little toxic to the cell culture and showed the great potential of CDs for fundamental biology research.

Table 2

The application of CDs-based sensor for analysis of water samples spiked with different concentrations of TNP.

Sample	Concentration of TNP (μM)		Recovery (%)	RSD (n=3, %)
	Amount added	Amount found		
Haihe River 1	5	4.79±0.05	95.8	1.04
2	10	10.82±0.13	108.2	1.20
Pool 1	5	4.63±3.81	92.6	0.82
2	10	10.51±0.22	105.1	2.09

Recovery=Amount founded/Amount added×100%.

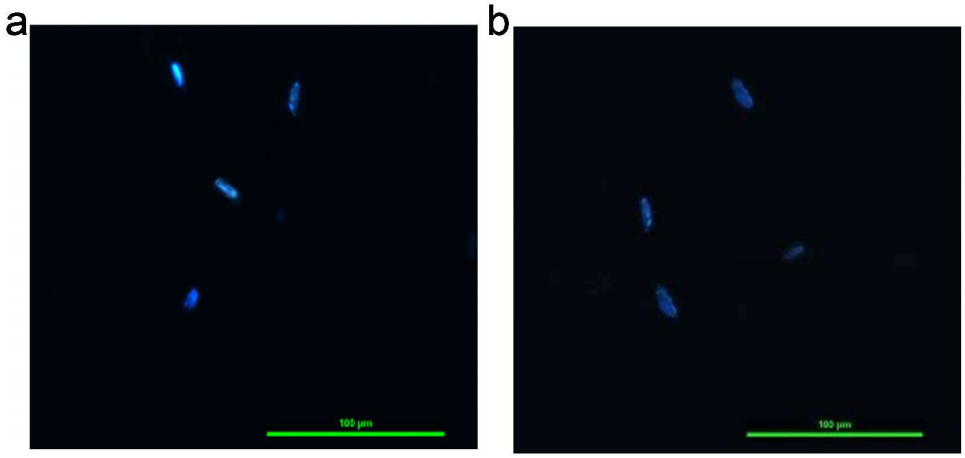

Fig. 7 Fluorescence microscopy images of E. coli after labeled with CDs for 2 h.

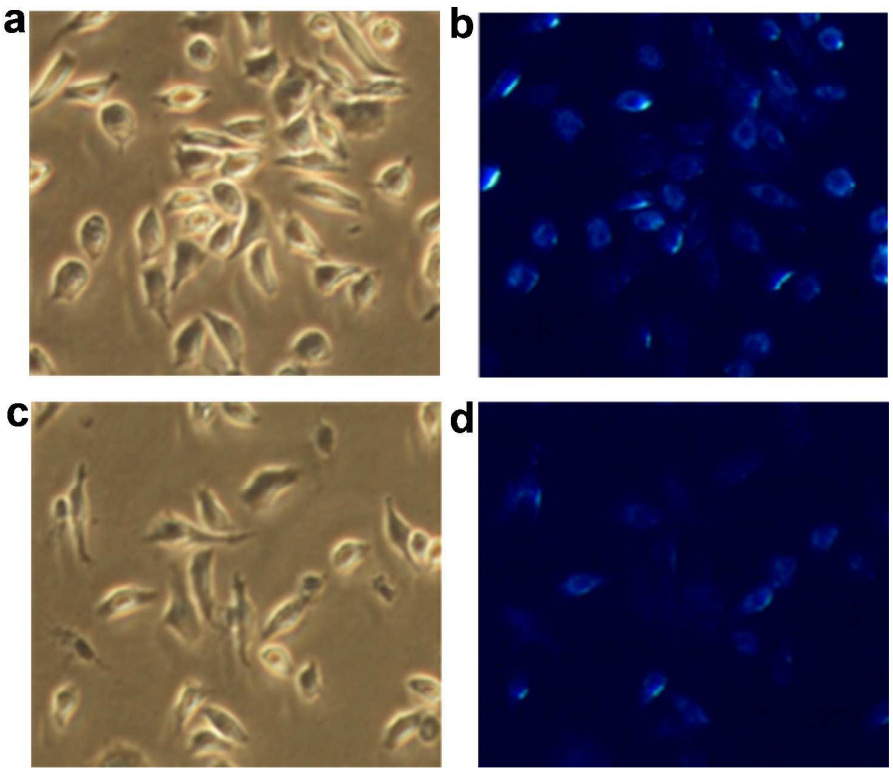

Fig. 8 Bright-field transmission image (a) and fluorescence image (b) of NIH-3T3 cells incubated with 10 μM CDs for 30 min at 37 ^{o}C. Bright-field transmission image (c) and fluorescence image (d) of NIH-3T3 cells which were first incubated with 10 μM CDs for 30 min and then incubated with 10 μM TNP for 30 min at 37 ^{o}C.

Conclusion

In conclusion, a simple and low toxicity method to use water-soluble CDs as nanosensor for the highly sensitive detection of trace TNP was presented. The as-prepared hydroxyl and carboxyl-rich CDs with uniformly spherical morphology and narrow size distribution were synthesized through the hydrothermal carbonization of phosphoric acid solution of sucrose. With the addition of TNP, a resonant energy transfer process between CDs and TNP was happened and thus the fluorescence intensity of CDs was obviously quenched. We optimized some important factors which may influence the sensing system. Under the optimum conditions, TNP could be detected with high sensitivity and low detection limit down to16.9 nM. Moreover, it exhibits good linear relationship between F0/F and the concentration of TNP in the wide concentration range of 0.2-17.0 μM. This sensing platform was successfully used to the detection of TNP in real water samples with satisfactory results. In addition, the novel method does not require further chemical modification of CDs and eliminates the necessity for organic dyes and organic solvent. In above sight, the accuracy and reliability of the present fluorescence method may pave a new way for designing optical sensor used to the determination of TNP.

Acknowledgements

The work described in this manuscript was supported by the National Natural Science Foundation of China (Nos. 21174103, 21374078) and Tianjin Research

Program of Application Foundation and Advanced Technology (No. 15JCYBJC18100).

References

[1] J. S. Yang and T. M. Swager, *J. Am. Chem. Soc.*, 1998, **120**, 11864.

[2] X. Deng, X. M. Huang and D. Wu, *Anal. Bioanal. Chem.*, 2015, **407**, 4607.

[3] M. Schaeferling, *Angew. Chem., Int. Ed.*, 2012, **51**, 3532.

[4] Y. Salinas, R. Martinez-Manez, M. D. Marcos, F. Sancenon, A. M. Costero, M. Parra and S. Gil, *Chem. Soc. Rev.*, 2012, **41**, 1261.

[5] J. Yinon, *Trends Anal. Chem.*, 2002, **21**, 292.

[6] Y. Ma, S. Huang and L. Wang, *Talanta*, 2013, **116**, 535.

[7] Y. Salinas, M. R. Martinez, M. D. Marcos, F. Sancenon, A. M. Castero, M. Parra and S. Gil, *Chem. Soc. Rev.*, 2012, **41**, 1261.

[8] J. M. Zhou, W. Shi, H. M. Li, H. Li and P. Cheng, *J. Phys. Chem. C*, 2014, **118**, 416.

[9] J. Akhavan (Ed), The Chemistry of Explosives, 2nd edition (The Royal Society of Chemistry, Cambridge, 2004) 21.

[10] S. Ebert, P. G. Rieger and A. J. Knackmuss, *J. Bacteriol.*, 1999, **181**, 2669.

[11] S. Kumar, N. Venkatramaiah and S. Patil, *J. Phys. Chem. C*, 2013, **117**, 7236.

[12] S. Shanmugaraju, S. A. Joshi and P. S. Mukherjee, *J. Mater. Chem.*, 2011, **21**, 9130.

[13] E. L. Holthoff, D. N. Stratis-Cullum and M. E. Hankus, *Sensors*, 2011, **11**, 2700.

[14] D. X. Ma, B. Y. Li, X. J. Zhou, Q. Zhou, K. Liu, G. Zeng and G. H. Li, *Chem. Commun.*, 2013, **49**, 8964.

[15] J. Xiao, L. Qiu, F. Ke, Y. Yuan, G. Xu, Y. Wang and X. Jiang, *J. Mater. Chem. A*,

2013, **1**, 8745.

[16] B. V. Harbuzaru, A. Corma, F. Rey, P. Atienzar, J. L. Jorda and H. Garcia, *J. Angew. Chem., Int. Ed.*, 2008, **47**, 1080.

[17] S. J. Toal and W. C. Trogler, *J. Mater. Chem.*, 2006, **16**, 2871.

[18] J. F. Wyman, M. P. Serve, D. W. Hobson, L. H. Lee and D. E. Uddin, *J. Toxicol. Environ. Health*, 1992, **37**, 313.

[19] B. H. Han, I. Manners and M. A. Winnik, *Chem. Mater.*, 2005, **17**, 3160.

[20] E. L. Holthoff, D. N. Stratis-Cullum and M. E. Hankus, Sensors, 2011, **11**, 2700.

[21] M. Berg, J. Bolotin and T. B. Hofstetter, *Anal. Chem.*, 2007, **79**, 2386.

[22] G. B. Demirel, B. Daglar and M. Bayindir, *Chem. Commun.*, 2013, **49**, 6140.

[23] S. S. Nagarkar, A. V. Desai and S. K. Ghosh, *Chem. Commun.*, 2014, **50**, 8915.

[24] L. M. Zhao, J. W. Ye, W. B. Li, R. F. Bogale, B. Wang, W. T. Gong and G. L. Ning, *Inorg. Chem. Commum.*, 2014, **46**, 212.

[25] V. Bhalla, A. Gupta and M. Kumar, *Org. Lett.*, 2012, **14**, 3112.

[26] T. Pazhanivel, D. Nataraj, V. P. Devarajan, V. Mageshwari, K. Senthil and D. Soundararajan, *Anal. Methods*, 2013, **5**, 910.

[27] B. Chen, F. Li, S. Li, W. Weng, H. Guo, T. Guo, X. Zhang, Y. T. Chen, X. Hong, S. You, Y. Lin, K. Zeng and S. Chen, *Nanoscale*, 2013, **5**, 1967.

[28] W. Kwon, S. Do, J. Lee, S. Hwang, J. K. Kim and S. W. Rhee, *Chem. Mater.*, 2013, **25**, 1893.

[29] L. Cao, M. J. Meziani, S. Sahu and Y. P. Sun, *Acc. Chem. Res.*, 2013, **46**, 171.

[30] H. Li, Z. Kang, Y. Liu and S. T. Lee, *J. Mater. Chem.*, 2012, **22**, 24230.

[31] J. C. G. Esteves da Silva and H. M. R. Goncalves, *Trends Anal. Chem.*, 2011, **30**, 1327.

[32] S. N. Baker and G. A. Baker, *Angew. Chem., Int. Ed.*, 2010, **49**, 6726.

[33] Y. Zou, F. Y. Yan, L. F. Dai, Y. M. Luo, Y. Fu, N. Yang and J. Y. Wun, *Carbon*, 2014, **77**, 1148.

[34] Y. Q. Dong, R. X. Wang, G. L. Li, C. Q. Chen, Y. W. Chi and G. Chen, *Anal. Chem.*, 2012, **84**, 6220.

[35] S. Qu, H. Chen, X. Zheng, J. Cao and X. Liu, *Nanoscale*, 2013, **5**, 5514.

[36] W. Shi, Q. Wang, Y. Long, Z. Cheng, S. Chen, H. Zheng and Y. Huang, *Chem. Commun.*, 2011, **47**, 6695.

[37] P. Wu and X. P. Yan, *Chem. Soc. Rev.*, 2013, **42**, 5489.

[38] H. T. Li, X. D. He, H. Huang, S. Y. Lian, Y. Liu, Z. H. Kang and S. T. Lee, *Carbon*, 2011, **49**, 605.

[39] S. Liu, J. Tian, L. Wang, Y. Zhang, X. Qin, Y. Luo, A. M. Asiri, A. O. Al-Youbi and X. Sun, *Adv. Mater.*, 2012, **24**, 2037.

[40] X. M. Yang, Y. Zhuo, S. S. Zhu, Y. W. Luo, Y. J. Feng and Y. Dou, *Biosens. Bioelectron.*, 2014, **60**, 292.

[41] M. J. Krysmann, A. Kelarakis, P. Dallas and E. P. Giannelis, *J. Am. Chem. Soc.*, 2011, **134**, 747.

[42] W. Shi, X. H. Li and H. M. Ma, *Angew. Chem.*, 2012, **124**, 6538.

[43] X. M. Yang, Y. Zhuo, S. S. Zhu, Y. W. Luo, Y. J. Feng and Y. Dou, *Biosens. Bioelectron.*, 2014, **60**, 292.

[44] J. H. Deng, Q. J. Lu, N. X. Mi, H. T. Li and M. L. Liu, *Chem. Eur. J.*, 2014, **20**, 4993.

[45] C. López, M. Zougagh, M Algarra, E. Rodríguez-Castellón, B. B. Campos, J. C. G. Esteves da Silva, J. Jiménez-Jiménez and A. Ríos, *Talanta.*, 2015, **132**, 845.

[46] Z. X. Huang, F. Lin, M. Hu, C. X. Li, T. Xu, C. Chen and X. Q. Guo, *J. Lumin.*, 2014, **151**, 100.

[47] A. M. Aslandaş, N. Balcı, M. Arık, H. Şakiroğlu, Y. Onganer and K. Meral, *Appl. Surf. Sci.*, 2015, **356**, 747.

[48] Q. Wu, W. Li, Y. J. Wu, Z. H. Huang and S. X. Liu, *Appl. Surf. Sci.*, 2014, **315**, 66.

[49] Q. Wang, S. R. Zhang, H. G. Ge, G. H. Tian, N. N. Cao and Y. Q. Li, *Sens. Actuators B: Chem.*, 2015, **207**, 25.

[50] E. S. Forzani, D. Lu, M. J. Leright, A. D. Aguilar, F. Tsow, R. A. Iglesias, Q. Zhang, J. Lu, J. Li and N. Tao, *J. Am. Chem. Soc.*, 2009, **131**, 1390.

[51] M. E. Germain and M. J. Knapp, *J. Am. Chem. Soc.*, 2008, **130**, 5422.

[52] M. M. Champion, E. A. Williams, G. M. Kennedy and P. A. Champion, *Mol. Cell. Proteomics.*, 2012, **11**, 596.

[53] M. A. Hahn, P. C. Keng and T. D. Krauss, *Anal. Chem.*, 2008, **80**, 864.

[54] X. L. Su and Y. Li, *Anal. Chem.*, 2004, **76**, 4806.

[55] S. Nandi, R. Malishev, K. Parambath Kootery, Y. Mirsky, S. Kolusheva and R. Jelinek, *Chem. Commun.*, 2014, **50**, 10299.

[56] L. Bao, Z. L. Zhang, Z. Q. Tian, L. Zhang, C. Liu, Y. Lin, B. P. Qi and D. W. Pang, *Adv. Mater.*, 2011, **23**, 5801.

[57] F. Wang, M. Kreiter, B. He, S. P. Pang and C. Y. Liu, *Chem. Comm.*, 2010, **46**, 3309.

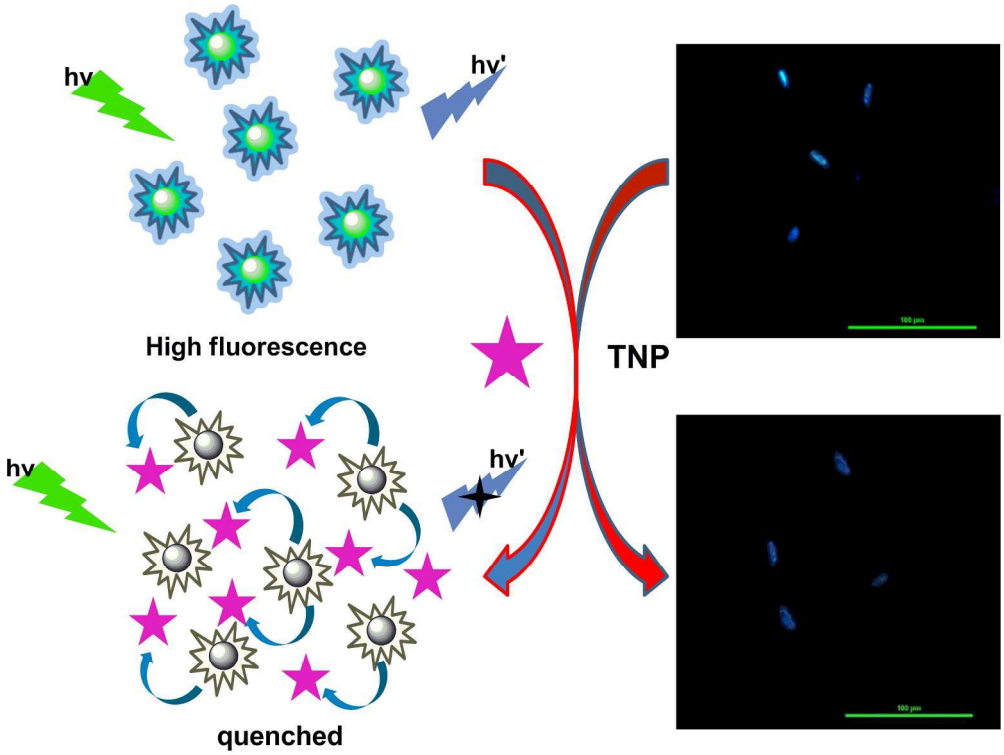

Graphical Abstract
221x168mm (300 x 300 DPI)